

# I Fundamentals



# 1

## The Impact of Electrocrystallization on Nanotechnology

*Georgi Staikov and Alexander Milchev*

### 1.1 Introduction

Electrocrystallization processes occurring at electrochemical solid/liquid interfaces have for a long time attracted the interest of many researchers from both fundamental and applied viewpoints. After the pioneering works of Max Volmer at the beginning of the last century [1, 2], the processes of electrocrystallization have been the subject of numerous intensive studies, the results of which have been reviewed in several books [3–7].

Electrocrystallization not only represents an interesting case of phase formation and crystal growth but is also a powerful method for various technological applications because the driving force of the process can be easily controlled by the current density and the electrode potential. Additional technological advantages over the vapor deposition techniques consist in the relatively low processing temperature and the high selectivity. The low temperature is important for systems in which undesirable interdiffusion between adjacent layers or structures can occur, whereas the high selectivity of electrocrystallization processes allows uniform modification of surfaces and structures with complicated profiles.

Phase formation and crystal growth phenomena are involved in many technologically important cathodic and anodic electrochemical reactions. The most frequently studied electrocrystallization process is cathodic metal deposition on foreign and native substrates from electrolytes containing simple and/or complex metal ions [3–25]. Typical examples are the electrocrystallization of Ag from Ag<sup>+</sup>-containing electrolytes [5, 7, 12–15, 21], the cathodic deposition of Ag on n-Si from electrolytes containing [Ag(CN)<sub>2</sub>]<sup>-</sup> ions [24], and the electrodeposition of Cu [3, 9, 17–20, 22, 25], which has recently become of significant technological importance for the fabrication of Cu interconnects on integrated circuit chips [26, 27].

A process widely used for preparation of metallic alloys and semiconducting compounds is cathodic codeposition from multicomponent electrolytes [28–39]. Typical examples are the electrochemical formation of Ni–Fe alloys by codeposition from Ni<sup>2+</sup>- and Fe<sup>2+</sup>-containing electrolytes [31] and the electrodeposition of n-type CdTe from electrolytes containing Cd<sup>2+</sup> and HTeO<sub>2</sub><sup>+</sup> ions [33]. Other impor-

tant electrocrystallization processes are anodic deposition of metal oxides and anodic oxidation of metals and semiconductors [23, 40–47]. The first type of processes can be illustrated by the anodic deposition of  $\text{PbO}_2$  from an aqueous  $\text{Pb}^{2+}$  solution [43]. The second type are substrate consuming processes, which occur in aqueous solution and usually start with adsorption of  $\text{OH}^-$  ions and place exchange reactions with the substrate [44]. Technologically important examples are the anodic oxidation of valve metals (Al, Nb, Ta, Ti) [45] and Si [46, 47].

The discovery of scanning tunneling microscopy and atomic force microscopy (STM and AFM) offered new exciting possibilities for *in situ* studies of the electrocrystallization phenomena down to an atomic level [48–50]. It would be not an overstatement to say that during the past two decades the application of these techniques has revolutionized the experimental work in this field and led to significant progress in the understanding of the atomistic aspects of electrocrystallization processes [5, 50–65]. The invention of scanning probe microscopy (SPM) also provoked a rapid development of the modern nanoscience and nanotechnology dealing with nanoscale structures and objects, including single atoms and molecules.

The application of electrocrystallization processes in nanotechnology requires a scaling down of the structures to the nanometer range. Therefore, in this chapter, we discuss some specific aspects of electrocrystallization, which are relevant for the electrochemical preparation and properties of various nanostructures. In Section 1.2 we compare the thermodynamic properties of large and small phases and introduce the concepts of supersaturation and the work for nucleus formation in electrochemical systems. The theoretical and experimental aspects of electrochemical nucleation and growth of nano-particles and ultrathin films are considered in Sections 1.3–1.5, whereas different approaches for localized electrocrystallization and preparation of nanostructures are discussed in Section 1.6. All considerations are illustrated with experimental results obtained in selected electrochemical systems.

## 1.2

### Thermodynamic Properties of Large and Small Phases

#### 1.2.1

##### The State of Thermodynamic Equilibrium

In order to describe the state of stable thermodynamic equilibrium we consider an electrochemical system consisting of an electrolyte solution of metal ions ( $\text{Me}^z$ ) with a valence  $z$  and an electrochemical potential  $\tilde{\mu}_{s, \infty}$ , an infinitely large metal crystal of the same material (Me) with an electrochemical potential  $\tilde{\mu}_{c, \infty}$  and an inert foreign substrate, which is used as a working electrode and whose Galvani potential  $\phi_{we, \infty}$  can be varied by means of an external source. For the purpose of this consideration we assume that the working electrode is polarized to the Galvani potential  $\phi_{c, \infty}$  of the bulk metal crystal. The temperature  $T$  is kept constant. The metal ions  $\text{Me}^z$  of the electrolyte may adsorb on the inert foreign substrate forming adatoms with an electrochemical potential  $\tilde{\mu}_{ad, \infty}$ . The equilibrium state of such

an electrochemical system is expressed through the equality of the electrochemical potentials  $\tilde{\mu}$  of the species within coexisting phases [5, 7, 15, 23]:

$$\tilde{\mu}_{s, \infty} = \tilde{\mu}_{c, \infty} = \tilde{\mu}_{ad, \infty} \quad (1.1)$$

where

$$\tilde{\mu}_{s, \infty} = \mu_s^0 + kT \ln a_{s, \infty} + ze\phi_{s, \infty} \quad (1.2)$$

$$\tilde{\mu}_{c, \infty} = \mu_c^0 + ze\phi_{c, \infty} \quad (1.3)$$

$$\tilde{\mu}_{ad, \infty} = \mu_{ad}^0 + kT \ln a_{ad, \infty} + ze\phi_{c, \infty} \quad (1.4)$$

In Eqs. (1.2)–(1.4),  $\mu_s^0$ ,  $\mu_c^0$  and  $\mu_{ad}^0$  are the standard state chemical potentials of the three species,  $a_{s, \infty}$ ,  $a_{c, \infty} = 1$  and  $a_{ad, \infty}$  are their activities and  $\phi_{s, \infty}$  and  $\phi_{c, \infty}$  are the corresponding Galvani potentials.

Making use of the equality  $\tilde{\mu}_{s, \infty} = \tilde{\mu}_{c, \infty}$  one obtains the Nernst equation,

$$E_{\infty} = E^0 + \frac{kT}{ze} \ln a_{s, \infty} \quad (1.5)$$

which gives the equilibrium potential  $E_{\infty} = \phi_{c, \infty} - \phi_{s, \infty}$  of a bulk metal crystal dipped in a solution of its ions with activity  $a_{s, \infty}$ . The standard potential  $E^0$  is defined by  $E^0 = (\mu_s^0 - \mu_c^0)/ze$ . The potential-activity ( $E - a_s$ ) diagram in Fig. 1.1 shows schematically the equilibrium curve corresponding to Eq. (1.5) and to the equality  $\tilde{\mu}_{s, \infty} = \tilde{\mu}_{c, \infty}$ .

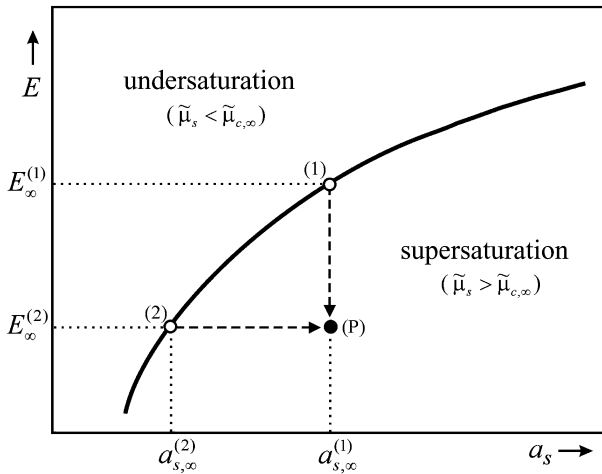


**Figure 1.1.** Schematic  $E(a_s)$  diagram for the equilibrium of a bulk metal crystal with its own ionic solution according to Eq. (1.5).

Another formula for the equilibrium potential  $E_{\infty}$  could be obtained also from the equilibrium condition  $\tilde{\mu}_{s, \infty} = \tilde{\mu}_{ad, \infty}$ . In that case for  $E_{\infty}$  it results,

$$E_{\infty} = \frac{\mu_s^0 - \mu_{ad}^0}{ze} + \frac{kT}{ze} \ln \left( \frac{a_{s, \infty}}{a_{ad, \infty}} \right) \quad (1.6)$$

and equating the two expressions for  $E_{\infty}$  yields a simple formula for the equilibrium adatoms' activity:  $a_{ad, \infty} = \exp[(\mu_c^0 - \mu_{ad}^0)/kT]$ . The same expression for  $a_{ad, \infty}$  follows from the equality of the electrochemical potentials  $\tilde{\mu}_{c, \infty}$  and  $\tilde{\mu}_{ad, \infty}$ .

### 1.2.2

#### Electrochemical Supersaturation and Undersaturation

In order to initiate either the growth of the bulk crystal or a process of nucleus formation on the inert foreign substrate it is necessary to supersaturate the parent phase, the electrolyte solution. This means to increase its electrochemical potential to a value  $\tilde{\mu}_s$  larger than that of the bulk new phase, the metal crystal ( $\tilde{\mu}_s > \tilde{\mu}_{c, \infty}$ ). Then it is the difference  $\Delta\tilde{\mu} = \tilde{\mu}_s - \tilde{\mu}_{c, \infty} > 0$ , which defines the *electrochemical supersaturation*.

In Fig. 1.1 the supersaturation range is situated below the equilibrium curve corresponding to Eq. (1.5). In the opposite case, when  $\tilde{\mu}_s < \tilde{\mu}_{c, \infty}$ , the difference  $\tilde{\mu}_s - \tilde{\mu}_{c, \infty} < 0$  defines the *electrochemical undersaturation*, which, if applied, would cause the electrochemical dissolution of the bulk crystal. Thus, the solid line in Fig. 1.1 indicates the stability limits of the infinitely large metal crystal.

As seen, the quantity  $\Delta\tilde{\mu}$  is the driving force of the two opposite types of electrochemical first order phase transition, either on a native or on a foreign substrate and therefore it is of fundamental and technological importance to express it by means of physical quantities, which can be easily measured and controlled.

The general formula for  $\Delta\tilde{\mu}$  that is most frequently used reads

$$\Delta\tilde{\mu} = ze\eta \quad (1.7)$$

where  $\eta$  is the *cathodic overpotential* defined either as<sup>1</sup>

$$\eta = E_{\infty} - E \quad (1.8)$$

or as

$$\eta = \frac{kT}{ze} \ln \frac{a_s}{a_{s, \infty}} \quad (1.9)$$

Equations (1.8) and (1.9) show that the parent phase can be supersaturated with respect to the bulk crystal in two different ways, as illustrated schematically

1) In this chapter, the cathodic overpotential is defined as a positive quantity.

in Fig. 1.1. In the first way, the solution activity  $a_s$  is kept constant at the value  $a_{s,\infty}^{(1)}$  and the state of the system is changed from the equilibrium point (1) to a point (P) located in the supersaturation range by changing the electrode potential from the equilibrium,  $E_{\infty}^{(1)}$ , to a more negative value  $E \equiv E_{\infty}^{(2)}$ . At this potential the bulk crystal should stay in equilibrium with a solution with an activity  $a_{s,\infty}^{(2)} < a_{s,\infty}^{(1)}$ . In the second way, the parent phase is supersaturated to the same state (P) but starting from the equilibrium state (2) and increasing the solution activity to a value  $a_s = a_{s,\infty}^{(1)}$  larger than the equilibrium value  $a_{s,\infty}^{(2)}$ , the electrode potential  $E$  being kept constant at  $E_{\infty}^{(2)}$ . As pointed out in Refs. [7, 66–68], this second possibility of applying the supersaturation allows one to invent a modified pulse potentiostatic technique, which has certain advantages, particularly when it is necessary to preserve the energy state of the electrode surface. The increase in supersaturation by increasing the activity of metal ions at constant electrode potential has also been applied successfully for development of polarization routines for localized electro-deposition of metal nanoclusters using the STM tip as a nanotool [56, 63, 69–72].

In the above considerations the electrochemical supersaturation was defined with respect to a 3D bulk metal phase. However, in the case of foreign substrates characterized by a strong *depositing metal–substrate* interaction, various expanded (gas-like) and/or condensed (solid-like) low-dimensional metal phases can be formed in the undersaturation range with respect to the 3D bulk metal phase, a phenomenon known as underpotential deposition (UPD) [5, 11, 56, 63]. The equilibrium potential of a condensed (solid-like) 2D metal phase can be expressed by [56]

$$E_{2D} = E_{\infty} - \frac{kT}{ze} \ln a_{2D} \quad (1.10)$$

Here  $a_{2D} < 1$  represents the activity of the 2D phase, which depends on the metal–substrate interaction. In this case the electrochemical supersaturation with respect to the condensed 2D metal phase is given by  $\Delta\tilde{\mu}_{2D} = ze\eta_{2D}$  where the cathodic overpotential is defined as  $\eta_{2D} = E_{2D} - E$ .

As already mentioned, the supersaturation may initiate both the process of nucleus formation on the foreign substrate and the growth of the bulk metal crystal, depending on which phase is switched on as a working electrode. In what follows we consider the two types of electrocrystallization phenomena.

### 1.2.3

#### The Thermodynamic Work for Nucleus Formation

The formation of an  $n$ -atomic nucleus of the new phase requires one to overcome a thermodynamic barrier  $\Delta\tilde{G}(n)$  called *nucleation work* and expressed by the general formula [5, 7, 12, 15]:

$$\Delta\tilde{G}(n) = -n\Delta\tilde{\mu} + \tilde{\Phi}(n) \quad (1.11)$$

Here  $\tilde{\Phi}(n)$  takes into consideration the total energy excess due to the creation of new interfaces when a nucleus appears on the electrode surface.

### 1.2.3.1 Classical Nucleation Theory

In the particular case of sufficiently large clusters the number of atoms  $n$  can be considered as a continuous variable and the quantity  $\tilde{\Phi}(n)$  could be expressed by means of the specific free *surface*, *interfacial* and *line* energies in the system *nucleus–electrolyte–working electrode*. In that case  $\Delta\tilde{G}(n)$  is a differentiable function and the condition for an extremum  $[d\Delta\tilde{G}(n)/dn]_{n=n_c} = 0$  yields [7, 15]

$$\Delta\tilde{\mu} = \left[ \frac{d\tilde{\Phi}(n)}{dn} \right]_{n=n_c} \quad (1.12)$$

Equation (1.12) represents a general expression for the Gibbs–Thomson equation giving us the interrelation between the supersaturation  $\Delta\tilde{\mu}$  and the size  $n_c$  of the so-called *critical nucleus*, which stays in unstable equilibrium with the supersaturated parent phase.

The inspection of the theoretical formula for the nucleation work shows that the  $\Delta\tilde{G}(n)$  versus  $n$  relationship displays a maximum at  $n = n_c$  (Fig. 1.2(a)), the values of  $\Delta\tilde{G}(n_c)$ ,  $n_c$  and  $\Delta\tilde{\mu}$  being interrelated according to

$$\Delta\tilde{G}(n_{c,3D}) = \frac{1}{3}\tilde{\Phi}(n_{c,3D}) = \frac{1}{2}n_{c,3D}\Delta\tilde{\mu} \quad (1.13)$$

when 3D clusters form on a foreign substrate and according to

$$\Delta\tilde{G}(n_{c,2D}) = \frac{1}{2}\tilde{\Phi}(n_{c,2D}) = n_{c,2D}\Delta\tilde{\mu} \quad (1.14)$$

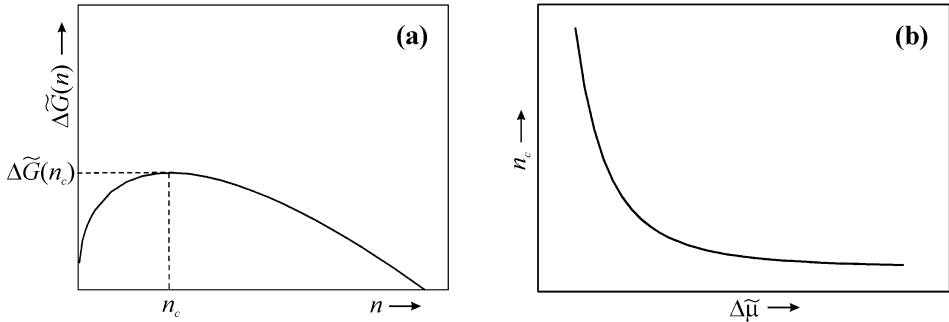


**Figure 1.2.** Dependence of the nucleation work  $\Delta\tilde{G}(n)$  on the cluster size  $n$  (a) and dependence of the critical nucleus size  $n_c$  on the supersaturation  $\Delta\tilde{\mu}$  (b) according to the classical nucleation theory (a schematic representation).

and

$$\Delta\tilde{G}(n_{c,2D}^*) = \frac{1}{2}\tilde{\Phi}(n_{c,2D}^*) = n_{c,2D}^*\Delta\tilde{\mu}_{2D} \quad (1.15)$$

when 2D clusters form on a native or on a foreign substrate, respectively. Figure 1.2(b) illustrates the supersaturation dependence of the critical nucleus size.

### 1.2.3.2 Atomistic Nucleation Theory

In the case of very small clusters the size  $n$  is a discrete variable and the macroscopic classical theory cannot be applied. Therefore the process of nucleus formation is described by means of atomistic considerations making use of the general formula for the nucleation work (Eq. (1.11)) [7, 15, 73, 74, 87]. The main result of the atomistic treatment is that the  $\Delta\tilde{G}(n)$  vs.  $n$  relationship is not a fluent curve but displays minima and maxima, depending on the structure and energy state of the cluster (Fig. 1.3(a)). The highest maximum at a given supersaturation corresponds to the critical nucleus size.

The discrete change in the size of the clusters at small dimensions also affects the  $n_c(\Delta\tilde{\mu})$  relationship. As seen from Fig. 1.3(b), in this case there corresponds to each critical nucleus a supersaturation interval and not a fixed value of  $\Delta\tilde{\mu}$  as predicted by the Gibbs–Thomson equation. These special properties of small clusters influence strongly the process of phase formation during electrocrystallization and have to be taken into consideration, particularly when interpreting experimental data for electrochemical nucleation on a foreign substrate. In that case the size of the critical nuclei does not exceed several atoms [5, 7, 12, 15, 17–25, 36–39, 75–84].

Apart from the purely thermodynamic analysis, the description of the nanoscale electrocrystallization phenomena requires special consideration of the kinetics of nucleus formation and the next section is devoted to this subject.

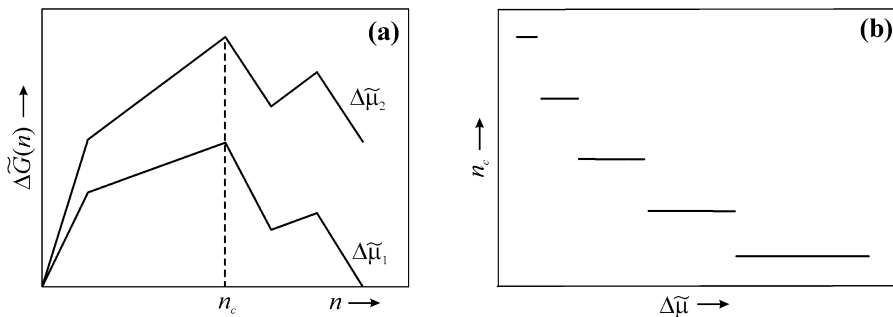


**Figure 1.3.** Dependence of the nucleation work  $\Delta\tilde{G}(n)$  on the cluster size  $n$  (a) and dependence of the critical nucleus size  $n_c$  on the supersaturation  $\Delta\tilde{\mu}$  (b) according to the atomistic nucleation theory (a schematic representation).

## 1.3

**Kinetics of Nucleus Formation in Electrocrystallization**

The nucleation work  $\Delta\tilde{G}(n_c)$  is a measure of the thermodynamic barrier, which has to be overcome in order to transform  $n_c$  ions from the electrolyte solution into an  $n_c$ -atomic nucleus of the new solid or liquid phase on the electrode surface. The rate  $J(t)$  of this process is a kinetic quantity and here we will comment upon its overpotential and concentration dependence in the case of a stationary nucleation when  $J(t)$  attains the constant value  $J_0$ .

The general theoretical formula for  $J_0$  reads [2, 85, 86]

$$J_0 = Z_0 W \lambda^{-1} \exp\left[-\frac{\Delta\tilde{G}(n_c)}{kT}\right] \quad (1.16)$$

where  $Z_0/\text{cm}^{-2}$  is the number density of active sites on the substrate,  $W/\text{s}^{-1}$  is the frequency of attachment of single atoms to the critical nucleus and  $\lambda^{-1}$  is a non-dimensional quantity accounting for the difference between the quasi-equilibrium and the stationary number of critical nuclei. In the macroscopic classical nucleation theory  $\lambda^{-1}$  is given as  $\lambda^{-1} = [\Delta\tilde{G}(n_c)/3\pi n_c^2 kT]^{1/2}$  and is called a ‘‘Zeldovich factor’’. It tends to unity at high supersaturations and/or very active substrates, when the critical nuclei are very small and their size remains constant over wide supersaturation intervals. For this typical case of electrochemical phase formation, particularly on foreign substrates, we shall reveal the overpotential and the concentration dependence of the stationary nucleation rate in terms of the atomistic theory of electrochemical phase formation [7, 15, 73, 87]. In this case the quantity  $W$  is given by

$$W = k_v \exp\left(-\frac{U}{kT}\right) \exp\left(-\frac{\alpha z e E}{kT}\right) \quad (1.17)$$

where  $k_v$  is a frequency factor,  $c$  is the concentration of metal ions,  $\alpha$  is the charge transfer coefficient and  $U$  is the energy barrier to transfer of an ion from the electrolyte to the critical nucleus at an electrode potential  $E = 0$ . This formula for  $W$  is suitable when the supersaturation  $\Delta\tilde{\mu}$  (Eq. (1.7)) is varied by changing the concentration of metal ions at a constant electrode potential  $E$  (Fig. 1.1), and substituting Eqs. (1.7), (1.9), (1.11) and (1.17) into Eq. (1.16) for the  $J_0(c)$  relationship at  $\lambda^{-1} \rightarrow 1$  one obtains [7, 68]:

$$J_0 = Z_0 \Omega(E) c^{n_c+1} \quad (1.18)$$

Here

$$\Omega(E) = k_v \left(\frac{\gamma}{\gamma_\infty c_\infty}\right)^{n_c} \exp\left[-\frac{U + \alpha z e E + \tilde{\Phi}(n_c)}{kT}\right] \quad (1.19)$$

where  $c_\infty$  is the equilibrium concentration of metal ions at the temperature  $T$  and  $\gamma$  and  $\gamma_\infty$  are the corresponding activity coefficients given as  $\gamma = a_s/c$  and  $\gamma_\infty = a_{s,\infty}/c_\infty$ . Thus Eq. (1.18) shows that the size  $n_c$  of the critical nucleus can be determined from an experimental  $J_0(c)$  relationship obtained at  $E = \text{const}$  according to [7, 68]:

$$n_c = \frac{d \ln J_0}{d \ln c} - 1 \quad (1.20)$$

In the case when the supersaturation is varied by varying the electrode potential  $E$  at a constant concentration  $c_\infty = \gamma_\infty a_{s,\infty}$  (Fig. 1.1) it turns out to be convenient to introduce the cathodic overpotential  $\eta = E_\infty - E$  in Eq. (1.17). Then accounting for the  $E_\infty(a_{s,\infty})$  relationship according to the Nernst equation (1.5) for the overpotential dependence of the stationary nucleation rate  $J_0$  at  $\lambda^{-1} \rightarrow 1$  one obtains [7, 68]:

$$J_0 = Z_0 \Omega(c_\infty) \exp \left[ \frac{(n_c + \alpha) z e \eta}{kT} \right] \quad (1.21)$$

where

$$\Omega(c_\infty) = k_v (\gamma_\infty c_\infty)^{1-\alpha} \exp \left[ - \frac{U + \alpha z e E^0 + \tilde{\Phi}(n_c)}{kT} \right] \quad (1.22)$$

As seen, in this case the size  $n_c$  of the critical nucleus can be determined from an experimental  $J_0(\eta)$  relationship obtained at  $c = c_\infty$  according to [7, 68]:

$$n_c = \frac{kT}{ze} \frac{d \ln J_0}{d \eta} - \alpha \quad (1.23)$$

Equations (1.16)–(1.23) are derived under the assumption of a constant number  $Z_0$  of active sites on the working electrode, which is a most simple example of electrochemical phase formation. In reality, the number of active sites could be a *time*, *potential* and *pH* dependent quantity [7, 66, 67].

## 1.4

### Energy State of the Electrode Surface and Spatial Distribution of Nanoclusters

The concept of “active sites” unavoidably raises the question about their physical nature and we should point out that the active sites are probably the most obscure characteristics of the nucleation kinetics. The reason is that, depending on the specific properties of the particular electrochemical system, the active sites may be entirely different nano-objects appearing on or disappearing from the electrode

surface due to various chemical and/or electrochemical reactions taking place prior to or simultaneously with the process of nucleus formation. These could be adsorption and desorption of organic and inorganic ions or molecules, surface transformations within preformed UPD layers, direct oxidation or reduction of the electrode surface etc. All this means that the assumption of an “inert” working electrode is certainly a serious approximation and a theoretical model of nucleus formation on a time-dependent number of active sites is developed in Refs. [7, 66, 67]. Without entering into detail we shall point out that if active sites appear on and disappear from the electrode surface as a result of an electrochemical reaction, parallel to the process of nucleus formation, the time dependence of the number  $N(t)$  of nuclei may be expressed by means of the following second-order differential equation [7, 66, 67]:

$$\frac{d^2N}{dt^2} + A \frac{dN}{dt} + B(N - N_0) = 0 \quad (1.24)$$

Here  $A$  and  $B$  depend on the nucleation frequency  $K_n = W\lambda^{-1} \exp[-\Delta\tilde{G}(n_c)/kT]$  and on the frequencies of appearance  $K_a^+$  and disappearance  $K_a^-$  of active sites to and from the electrode surface.  $N_0 = Z_a^0 + Z_l^0$  is the total number of active sites at time  $t = 0$ ,  $Z_a^0$  and  $Z_l^0$  being the numbers of the available and of the latent active sites at the time moment  $t = 0$ .

Exact analytical solution of Eq. (1.24) is possible and yields theoretical expressions for the nucleation rate  $J(t) = dN(t)/dt$  and for the number of nuclei  $N(t)$  in the case of a time-dependent number of active sites. Figure 1.4 illustrates the obtained result and shows that the nucleation rate has a non-zero initial value

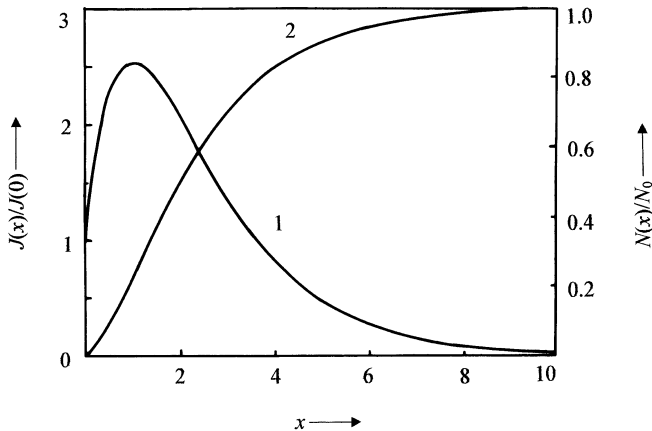


**Figure 1.4.** Non-dimensional plots  $J(x)/J(0)$  (1) and  $N(x)/N_0$  (2) versus  $x = t/t_m$  calculated according to the theoretical model of nucleus formation on a time-dependent number of active sites [7, 66, 67].

$J(0) = (dN/dt)_{t=0} = K_n Z_a^0$ , a zero final value,  $J(\infty) = 0$ , and displays a maximum, at time  $t = t_m$ . As for  $N(t)$  it changes from zero to the maximal value  $N_0 = Z_a^0 + Z_i^0$  at sufficiently long times when all latent active sites are developed and occupied by the nuclei of the new phase.

The detailed theoretical analysis carried out in Refs. [7, 66, 67] shows that, in this complex case of electrochemical phase formation, a stationary state may be established only under special circumstances and after a certain induction period. It turns out, also, that the quantity which we use to measure and to call a *stationary nucleation rate* may provide experimental information not on the *nucleation* kinetics but on the kinetics of *appearance of active sites* on the electrode surface, if this process is the rate determining step in the initial stage of the phase transition. This finding must be taken into consideration when interpreting experimental data on the kinetics of nucleus formation, both on foreign and on native substrates.

An important question closely related to the nucleation kinetics concerns the location of nuclei on the electrode surface. In particular, it turns out to be important for many practical purposes to know whether nanoclusters are randomly distributed on the substrate or whether there is a certain *cluster-cluster* correlation. The most frequently used approach to this problem consists in the statistical analysis of the distances between nearest neighbor clusters and comparison of the obtained results with theoretical formulae based on the Poisson law for a purely random distribution [88, 89]. Here we present some experimental data interpreted by means of the general theoretical expression for the probability distribution function  $dP_{v,n}$  of the distances between  $n$ th neighbor clusters randomly located within a  $v$ -dimensional space, derived in Ref. [90]:

$$dP_{v,n} = \frac{v}{(n-1)!} \left[ \frac{\pi^{v/2} N_{0,v}}{\Gamma(1+v/2)} \right]^n r_{v,n}^{n-1} \exp \left[ -\frac{\pi^{v/2} N_{0,v} r_{v,n}^v}{\Gamma(1+v/2)} \right] dr_{v,n} \quad (1.25)$$

In fact Eq. (1.25) gives us the probability  $dP_{v,n}$  for a given cluster to have its  $n$ th neighbor at a distance between  $r_{v,n}$  and  $r_{v,n} + dr_{v,n}$  and in it  $N_{0,v}$  is the average cluster density,  $\Gamma$  is the gamma function and  $v$  is the space dimension. Thus  $v = 1$  if clusters are formed on a step,  $v = 2$  if clusters are formed on a surface and  $v = 3$  if clusters are incorporated within a three-dimensional matrix, e.g. within the bulk of an electrically conducting medium. Correspondingly, the average distance  $\bar{r}_{v,n}$  between clusters is defined as

$$\bar{r}_{v,n} = \int_0^{\infty} r_{v,n} dP_{v,n} \frac{\Gamma(n+1/v)}{(n-1)!} \left[ \frac{\Gamma(n+v/2)}{\pi^{v/2} N_{0,v}} \right]^{1/v} \quad (1.26)$$

Figure 1.5 illustrates the correlation between the experimental (histograms) and theoretical (lines) distributions of the distances between first, second and third neighbor silver crystals electrodeposited on a mechanically polished glassy carbon electrode [91]. As seen, in all cases the experimentally measured smallest distances appear with a probability lower than theoretically predicted for a random distribu-

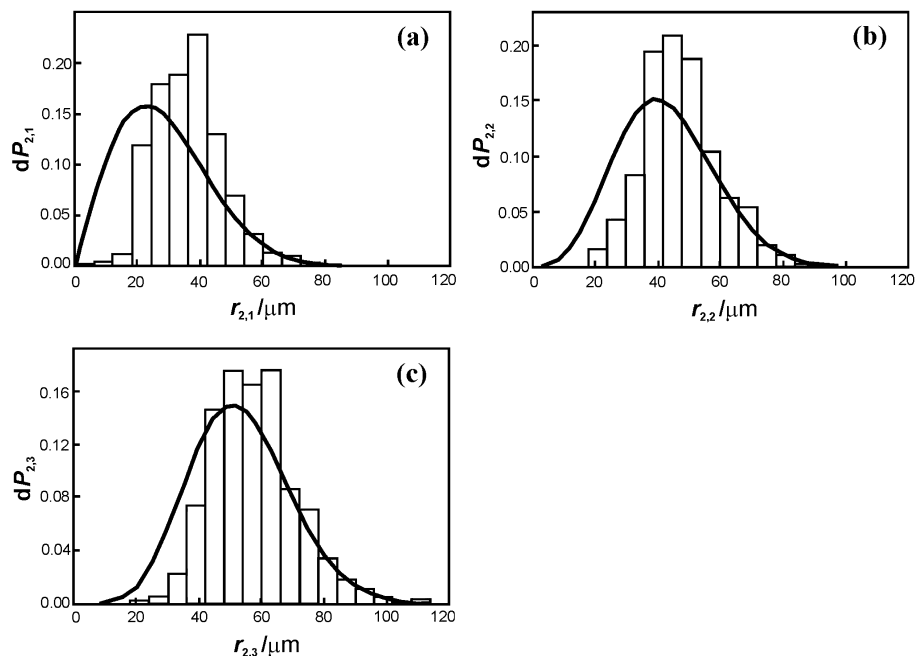


**Figure 1.5.** Experimental (histograms) and theoretical (lines) distribution of the distances between *first* (a), *second* (b) and *third* (c) neighbor silver crystals electrochemically deposited on a flat glassy carbon electrode,  $N_{0,2} = 2.75 \times 10^4 \text{ cm}^{-2}$  [91].

tion, the effect being less pronounced for second and for third neighbor clusters. This should mean that zones of reduced nucleation rate arise around the growing stable clusters, of course, if we assume that the active sites themselves are randomly distributed on the electrode surface. This has been proven to be the case for the mechanically polished glassy carbon working electrode [91]. However, it might not necessarily be true for other amorphous or crystalline substrates.

Deviations from the random distribution were experimentally registered also in other electrochemical systems [76, 79, 92–95] and were also confirmed by means of computer simulations [96, 97]. In the next section we consider the electrochemical growth of nanoclusters and comment upon the physical nature of the zones of reduced nucleation rate.

## 1.5

### Electrochemical Growth of Nanoparticles and Ultrathin Films

The growth kinetics of three- and two-dimensional (3D and 2D) clusters have been examined by many authors and under different experimental conditions account-

ing for various limitation factors (see e.g. Refs. [3–8] and the literature cited therein). Here we present briefly only the basic theoretical and experimental findings.

### 1.5.1

#### Growth of 3D Nanoclusters

At a constant overpotential  $\eta$  the current  $I_1(t)$  of a single hemispherical cluster growing under the conditions of combined charge transfer and diffusion limitations is given by [98]:

$$I_1(t) = p \left[ \frac{1 + nt}{(1 + 2nt)^{1/2}} - 1 \right] \quad (1.27)$$

In Eq. (1.27)

$$p = \frac{4\pi(zFDc_\infty)^2}{i_0} \left\{ \exp\left(-\frac{\alpha zF\eta}{RT}\right) - \exp\left[-\frac{(1 + \alpha)zF\eta}{RT}\right] \right\} \quad (1.28)$$

$$n = \frac{V_M i_0^2}{(zF)^2 D c_\infty} \left\{ \exp\left(\frac{2\alpha zF\eta}{RT}\right) - \exp\left[-\frac{(1 - 2\alpha)zF\eta}{RT}\right] \right\} \quad (1.29)$$

where  $D$  is the diffusion coefficient of metal ions and  $i_0$  is the exchange current density at the *cluster–solution* interface boundary.

The growth of a single cluster affects significantly both the concentration and the overpotential distribution in the cluster vicinity [96, 99, 100]. Thus the concentration  $c(\rho)$  and the overpotential  $\eta(\rho)$  at a distance  $\rho$  from the cluster are given by:

$$c(\rho) = c_\infty \left[ 1 - \frac{I_1(t)}{2\pi\rho zFDc_\infty} \right] \quad (1.30)$$

$$\eta(\rho) = \eta + \frac{RT}{zF} \ln \left[ 1 - \frac{I_1(t)}{2\pi\rho zFDc_\infty} \right] \quad (1.31)$$

and substituting these two formulae into Eq. (1.21), for the stationary nucleation rate  $J_0(\rho)$  at a distance  $\rho$  one obtains

$$J_0(\rho) = J_0 \left[ 1 - \frac{I_1(t)}{2\pi\rho zFDc_\infty} \right]^{n_c+1} \quad (1.32)$$

The solid line in Fig. 1.6 illustrates the non-dimensional distribution of the stationary nucleation rate around a growing hemispherical cluster, if the single atom adsorbed on the electrode surface is a critical nucleus ( $n_c = 1$ ) within the entire zone of reduced concentration and overpotential. However, since the critical nucleus size is a function of the overpotential  $\eta(\rho)$  it appears that, in the general case, different clusters may play the role of critical nuclei in the vicinity of the growing

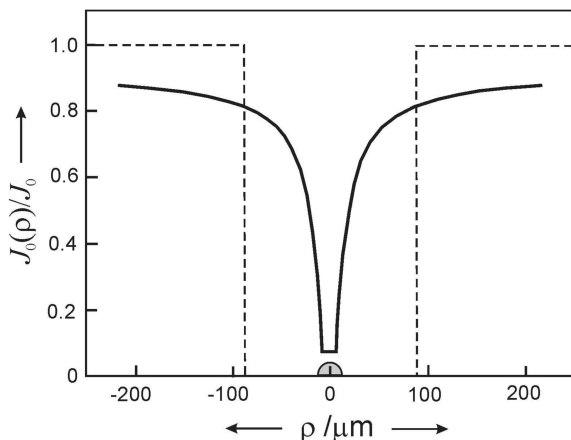


**Figure 1.6.** Cross section of a non-dimensional distribution of the stationary nucleation rate around a spherical cluster for the case  $n_c = 1$  atom (—). Profile of a planar nucleation exclusion zone (---).

supercritical one and this yields much more complex distribution of the nucleation rate [7, 101].

If *multiple* hemispherical clusters form and grow on the electrode surface then the local zones of reduced nucleation rate spread out and gradually overlap, which means that a general theoretical model describing the overall nucleation kinetics should account for the collective interaction between a large number of growing clusters. The problem has no exact solution and a most frequently employed approximation is based on the idea of overlapping *planar diffusion zones* in which nucleation is fully arrested [14, 102–106] (Fig. 1.6). Thus, in the case of growth of clusters under the conditions of complete diffusion control, for the total current one obtains:

$$i_N(t) = \beta zFc \left(\frac{D}{\pi t}\right)^{1/2} \left\{ 1 - \exp\left[-\frac{1}{2}J_0\pi(8\pi cV_M)^{1/2}Dt^2\right] \right\} \quad (1.33)$$

if  $N(t)$  clusters are *progressively* formed on the electrode surface during the time interval  $(0, t)$  and

$$i_{N_0}(t) = zFc \left(\frac{D}{\pi t}\right)^{1/2} \left\{ 1 - \exp[-N_0\pi(8\pi cV_M)^{1/2}Dt] \right\} \quad (1.34)$$

if  $N_0$  clusters appear *instantaneously* at the initial moment  $t = 0$ . In Eq. (1.33)  $\beta$  is a numerical constant, which equals 1 according to Refs. [14, 102] and 4/3 according to Refs. [105, 106].

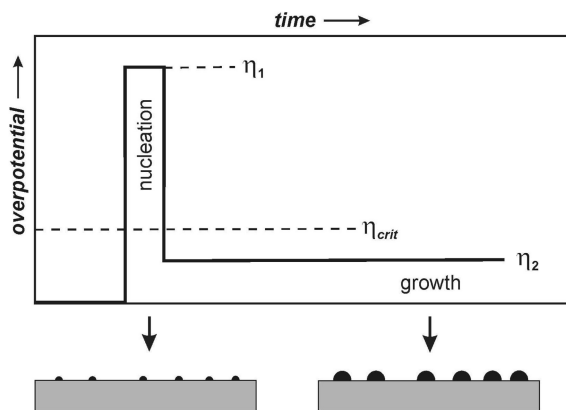


**Figure 1.7.** Schematic representation of the double-pulse polarization routine for preparation of metal nanoparticles and compact metal films.

A specific feature of electrochemical nucleation is the existence of an overpotential threshold (“critical overpotential”  $\eta_{crit}$ ) below which the nucleation rate  $J_0$  is practically zero and above which it raises exponentially (cf. Eq. (1.16)) [1–8]. Based on this feature an efficient double-pulse polarization routine for metal electrodeposition was developed, as illustrated schematically in Fig. 1.7 (see e.g. Refs. [5, 7] and the references cited therein).

The double-pulse technique allows the formation, either *progressively* or *instantaneously*, of a large number of metal clusters during the first short pulse at  $\eta_1 \gg \eta_{crit}$ . This pulse is followed by a second one of a much lower cathodic overpotential  $\eta_2 \ll \eta_{crit}$  during which only further growth of clusters is possible. This polarization routine has been successfully applied both for electrodeposition of metal nanoparticles with a narrow size distribution [107, 108] and for electroplating of compact thin metal films [20, 109, 110].

### 1.5.2

#### Growth of 2D Nanoclusters and Formation of UPD Monolayers

As already mentioned in Section 1.2.2, in systems characterized by strong interaction energy between the depositing metal and the foreign substrate the deposition of the bulk metal phase can be preceded by UPD of different low-dimensional metal or alloy phases [5, 11, 51–65, 111–121]. In such systems, at potentials close to the equilibrium potential  $E_\infty$ , the foreign substrate is usually covered by condensed UPD monolayers, which can be either commensurate or incommensurate, depending on the crystallographic *deposit–substrate* misfit.

Figures 1.8 and 1.9 illustrate the evolution of surface morphology during the UPD of condensed Ag and Pb monolayers on stepped Au(100) and Ag(111) substrates, respectively [5, 56, 63, 111, 114–117, 120]. As seen in Fig. 1.8, the con-

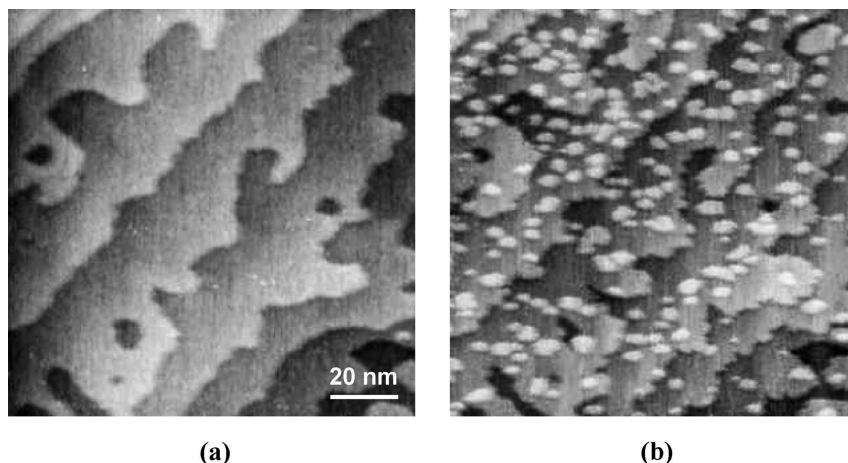


**Figure 1.8.** UPD of Ag on a stepped Au(100) substrate. Electrolyte: 5 mM  $\text{Ag}_2\text{SO}_4 + 0.1 \text{ M H}_2\text{SO}_4$  ( $T = 298 \text{ K}$ ). (a) *in situ* STM image of the substrate surface at underpotential  $E - E_\infty = 400 \text{ mV}$ . (b) *in situ* STM image showing the formation of a condensed Ag monolayer at underpotential  $E - E_\infty = 15 \text{ mV}$ .

densified Ag monolayer on Au(100) is formed by multiple nucleation and growth of 2D Ag clusters occurring simultaneously at monatomic steps and on flat terraces [116, 117]. The STM imaging with atomic resolution shows that the condensed Ag monolayer is commensurate, as expected because of the very low Ag–Au misfit. In contrast to this, a compressed close-packed incommensurate Pb monolayer is

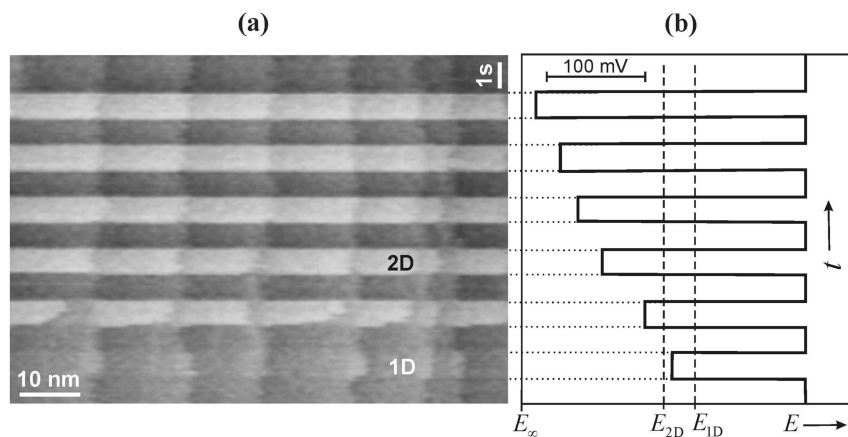


**Figure 1.9.** UPD of Pb on a stepped Ag(111) substrate. Electrolyte: 5 mM  $\text{Pb}(\text{ClO}_4)_2 + 0.5 \text{ M Na}(\text{ClO}_4)_2 + 5 \text{ mM HClO}_4$  ( $T = 298 \text{ K}$ ). (a) *in situ* AFM image showing the 1D and 2D Pb phase formation (b) applied polarization routine.

formed on Ag(111) due to the significant Pb–Ag misfit [5, 56, 63, 111, 115, 116, 120]. Figure 1.9 shows that in this case the formation of the condensed Pb monolayer (2D Pb phase) starts exclusively at substrate monatomic steps. The linescan ( $x-t$ ) AFM image indicates also that the monolayer growth is preceded by a decoration of the monatomic steps and formation of a “1D Pb phase” occurring at potentials more positive than the equilibrium potential  $E_{2D}$  of the condensed 2D Pb phase. These observations clearly show that substrate monatomic steps play an important role in the formation of condensed UPD monolayers and have to be taken into account in the theoretical models describing the kinetics of 2D nucleation and growth [56].

As a surface limited process, UPD offers attractive possibilities for surface modification on an atomic scale and preparation of nanomaterials with unconventional chemical and physical properties. Some important examples are summarized schematically in Fig. 1.10. Underpotential codeposition from multicomponent electrolytes is used successfully in the so-called “electrochemical atomic layer epitaxy” (EC-ALE) for a nanoscale controlled preparation of different superlattices and ultrathin films of metals, alloys and semiconducting compounds, as illustrated schematically in Fig. 1.10(a) and (b) [5, 51, 61, 122–124]. Another interesting application of the UPD phenomena is to use an UPD metal layer as a surfactant influencing the kinetics and mechanism of electrochemical growth of a more noble metal [125–128]. In this case, the UPD metal layer floats on the surface of the growing noble metal (Fig. 1.10(c)) and the growth process involves a place-exchange between the depositing metal atoms and the atoms of the UPD layer. It

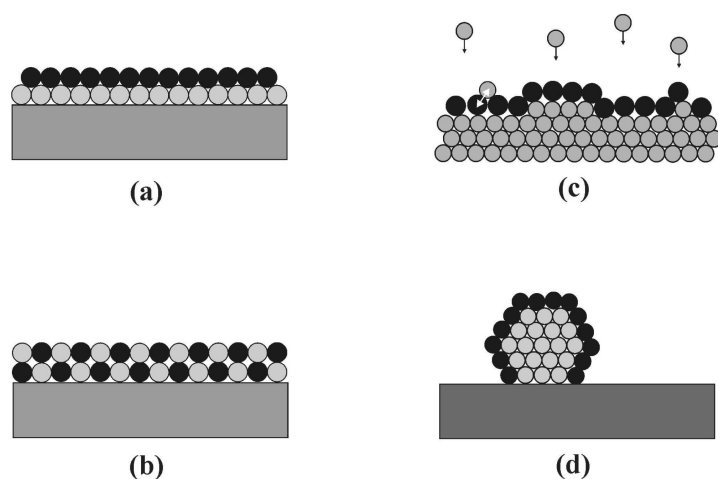


**Figure 1.10.** Possible applications of UPD in nanotechnology (a schematic representation). (a) deposition of superlattices and multilayers, (b) deposition of ultrathin alloy and compound films, (c) electrochemical surfactant mediated growth, (d) monolayer modification of nanoparticles.

was demonstrated that the use of Pb as a surfactant in the electrochemical deposition of Ag on Ag(111) and Au(111) facilitates a layer-by-layer growth mode [125, 126]. Recently Pb and Tl were used successfully as surfactants enhancing the electrodeposition rate of Au in order to achieve a “superfill” (perfect filling) of nano-sized trenches according to the so-called “curvature enhanced accelerator coverage” (CEAC) mechanism [127, 128]. As illustrated in Fig. 1.10(d), the UPD process can be applied also for surface modification of metal nanoparticles by a monolayer of a second metal [129–131]. The use of substrates such as graphite or glassy carbon, which are inert with respect to metal UPD, is suitable in this case. Noble metal nanoparticles with a controlled size can be electrodeposited on the inert substrate and selectively modified by a subsequent UPD of a less noble metal [131]. Recently such UPD modification was used as an intermediate step in a new technique for preparation of novel electrocatalysts based on Pt monolayers deposited on the surfaces of carbon-supported non-noble metal/noble metal (core/shell) nanoparticles (Ni/Au, Co/Pd and Co/Pt) [132]. In this technique the Pt monolayer is deposited by galvanic displacement of a pre-deposited Cu UPD monolayer. The Pt monolayer electrocatalysts prepared by this technique are characterized by a mass activity higher than that of the commercial Pt-containing catalytic materials [132].

## 1.6

### Localization of Electrocrystallization Processes and Nanostructuring

An important property of electrocrystallization is its high selectivity. This property offers numerous possibilities for localization of electrocrystallization processes and preparation of nanostructures for fundamental research and technological applications. A widely applied method for localized electrocrystallization is based on the use of insulating templates such as lithographically patterned resist layers or nanoporous membranes (see e.g. Refs. [133, 134], Chapter 3 in this book and the references cited therein). The modification of a conducting substrate with an insulating template results in the formation of negative (recessed) structures. A single negative structure of this type is shown schematically in Fig. 1.11. For the filling of such a structure by electrodeposition, its aspect ratio  $h/d$  (depth/diameter) and the surface state of the conducting substrate are important. As already discussed in Section 1.4, the energy state of the substrate surface determines the density of active nucleation sites  $Z_0$  and the nucleation rate  $J_0$ . The initial stages of localized electrocrystallization in the negative structure can be characterized by the mean nucleation time  $\bar{\tau}_n = \frac{1}{J_0\pi(d/2)^2}$  and the mean time  $\bar{\tau}_L = \frac{d}{V_L}$  needed for the first cluster to cover the bottom surface of the structure. Here  $\pi(d/2)^2$  and  $V_L$  represent the bottom area of the structure and the lateral growth rate of the crystalline cluster, respectively. Two different growth modes can generally be distinguished, depending on the electrocrystallization conditions, as illustrated schematically in Fig. 1.11: (i) a *mononuclear growth mode* occurring at  $\bar{\tau}_n \gg \bar{\tau}_g$  through the formation and growth

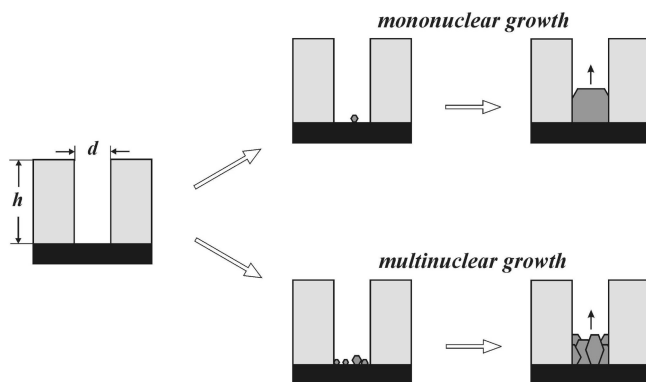


**Figure 1.11.** Mono- and multinuclear growth modes in a negative insulator/conductor structure (a schematic representation).

of a single nucleus and (ii) a *multinuclear growth mode* occurring at  $\bar{\tau}_n \ll \bar{\tau}_g$  through the formation and growth of a large number of crystalline nuclei. The localized electrocrystallization by the mono- or multinuclear growth mode can be applied successfully for the fabrication of single- or polycrystalline metal nanowires with extremely high aspect ratios, as demonstrated recently using nanoporous polymer membranes as templates [135, 136]. Another approach to the preparation of various metal and compound nanowires is based on the preferred electrocrystallization at step edges (see e.g. Refs. [108, 137–139] and Chapter 9 in this book).

The invention of scanning probe microscopy (SPM) opened a new window not only for *in situ* surface studies of electrode surfaces at an atomic scale but also for the local nanostructuring and modification of surfaces by electrochemical phase formation using the SPM tip as a nanoelectrode (cf. Fig. 1.12(a)). In this case the ratio between the polarization resistance  $R_{pol}$  (including the resistances for the charge transfer through the new formed phase and interfaces) and the electrolyte resistance  $R_{el}$  in the electrochemical *in situ* SPM cell [140–142] is crucial for the localization. Electrochemical phase formation can be localized if  $R_{pol} \ll R_{el}$  (cf. Fig. 1.12(b)). Such localized electrocrystallization was successfully realized by means of *in situ* STM in the case of metal electrodeposition from dilute electrolyte solutions (see e.g. Refs. [56, 63, 69–72] and Chapter 6 in this book). For  $R_{pol} \gg R_{el}$ , however, the formation of the new phase in the electrochemical *in situ* SPM cell becomes fully delocalized. Thus, no localized formation of insulating anodic oxides could be achieved by *in situ* SPM, even in pure water, due to the very high resistance of the oxide phases ( $R_{pol} \gg R_{el}$ ). In this case the localization of the oxidation process can be realized by *ex situ* SPM in a humid atmosphere. Under these conditions the water vapors condense between the SPM tip and the substrate forming a water meniscus, which acts as electrolyte and localizes the electrochemical oxidation (Fig. 1.13a). This approach is widely used for preparation of various nanostruc-

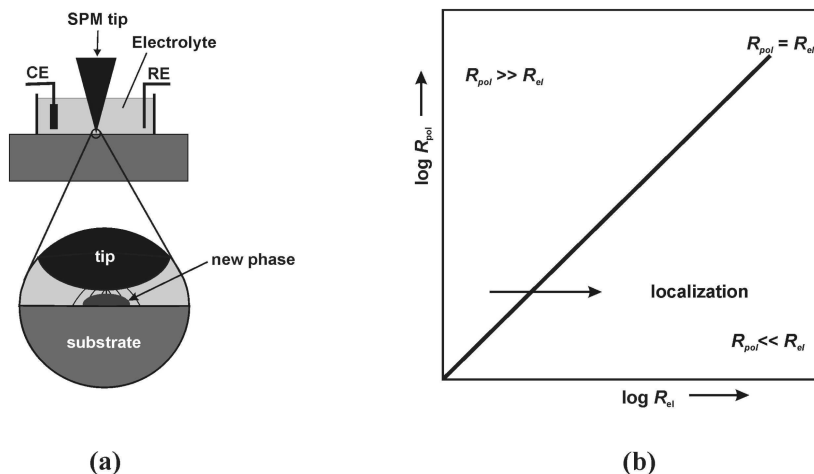


**Figure 1.12.** (a) Schematic representation of localized electrodeposition in the *in situ* SPM cell. (b) Schematic  $\log R_{pol} - \log R_{el}$  plot showing the localization conditions.

tures by local AFM tip-induced anodic oxidation of semiconductors and valve metals [23, 46, 140–148]. Figure 1.13(b) shows, as an example, a pattern composed of linear oxide structures fabricated by scanning a conducting AFM tip on a p-Si substrate in humid air [142]. The height and the width of the oxide structures depend on the applied bias voltage  $\Delta U$ , the scan rate of the AFM tip and the relative humidity of the atmosphere. Figures 1.14(a) and (b) show the voltage dependence

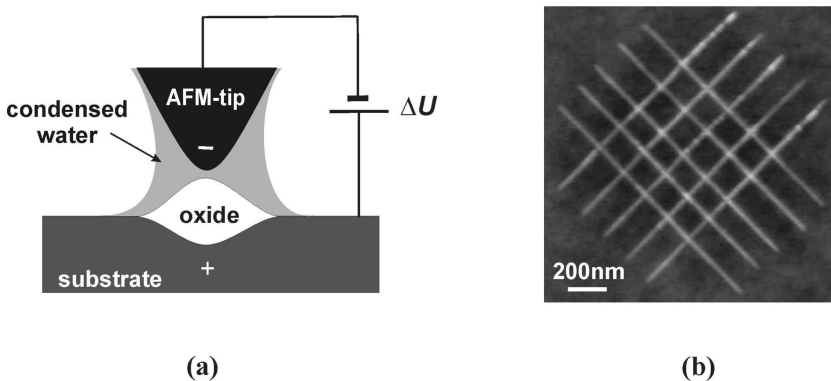


**Figure 1.13.** Localized anodic oxidation induced by the AFM tip. (a) Schematic representation of the electrochemical nanocell formed between the AFM tip and the substrate in humid atmosphere. (b) SiO<sub>2</sub> pattern fabricated by local AFM tip-induced oxidation of p-Si(111) (bias voltage  $\Delta U = 8.5$  V, tip scan rate  $200 \text{ nm s}^{-1}$ , relative humidity 3%).

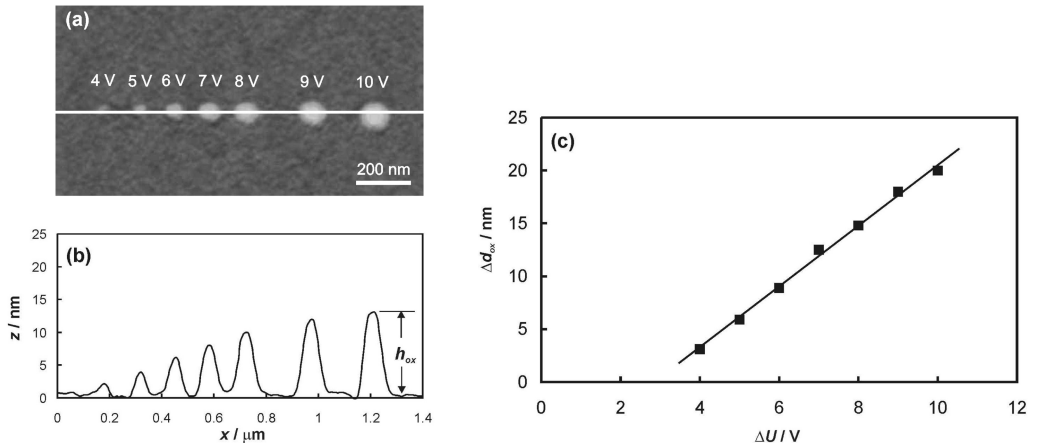


**Figure 1.14.** (a)  $\text{Nb}_2\text{O}_5$  dots generated on a 20 nm thick Nb film by a fixed AFM tip applying different bias voltages  $\Delta U$  (polarization time  $t_p = 10$  s, relative humidity 40%). (b) Single line section of the AFM image in (a). (c)  $\Delta d_{\text{ox}} - \Delta U$  dependence derived from (b).

of  $\text{Nb}_2\text{O}_5$  dots generated by localized anodic oxidation of a thin Nb film at fixed AFM tip position (point oxidation) and constant polarization time. The anodic oxidation of Nb is a substrate-consuming electrode reaction ( $2\text{Nb} + 5\text{H}_2\text{O} \rightarrow \text{Nb}_2\text{O}_5 + 10\text{H}^+ + 10\text{e}^-$ ), in which two moles Nb are needed for the formation of one mole  $\text{Nb}_2\text{O}_5$ . Thus, the increase in the thickness  $\Delta d_{\text{ox}}$  of the generated oxide dots can be estimated from their height  $h_{\text{ox}}$  (cf. Fig. 1.14(b)) using the relation  $\Delta d_{\text{ox}} = 1.56h_{\text{ox}}$  where the factor 1.56 is determined by the molar volumes of Nb and  $\text{Nb}_2\text{O}_5$  [140]. The derived linear  $\Delta d_{\text{ox}} - \Delta U$  dependence shown in Fig. 1.14(c) is in good agreement with the high-field law of the oxide growth [23, 45].

The preparation of lateral metal–insulator–metal (MIM) structures by local oxidation is of particular interest for nanoelectronics. Thus it is essential to find optimal conditions for a complete AFM tip-induced local oxidation of a thin metal film. Figure 1.15 shows an experimental routine, which has been used to control the complete local oxidation of a 5 nm thick Nb film sputtered on a thermally-oxidized silicon substrate [140]. Square structures were first fabricated with a scan rate of the AFM tip of  $200 \text{ nm s}^{-1}$  and bias voltages  $\Delta U$  ranging between 6 and 12 V (Fig. 1.15(a)). In a second step, an attempt was made for a local oxidation of Nb along a 500 nm line inside each square structure in order to check if there is still an electric contact between Nb film inside and outside each square structure (Fig. 1.15(b)). The results obtained show that under the given experimental conditions a complete oxidation of the thin Nb film can be achieved at bias voltages higher than 10 V. The generated structures are presented schematically in Fig. 1.15(c). This approach can be applied successfully for the fabrication of different lateral MIM structures by local AFM tip-induced nanooxidation of ultrathin films of valve metals.

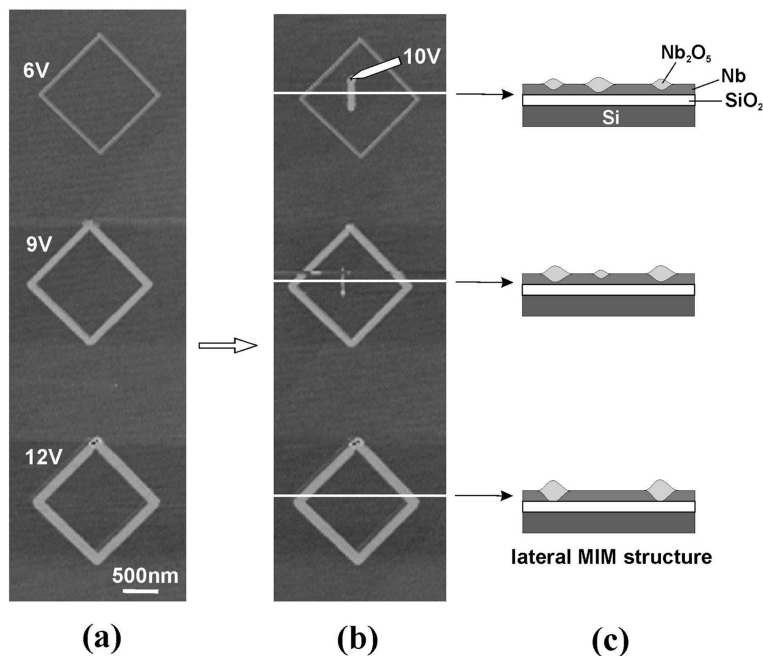


**Figure 1.15.** Experimental routine used for checking the complete local oxidation of a Nb thin film (Nb film thickness 5 nm, AFM tip scan rate  $200 \text{ nm s}^{-1}$ , relative humidity 40%). (a)  $\text{Nb}_2\text{O}_5$  structures prepared by tip-induced oxidation with different bias voltages. (b) AFM image obtained after an attempt for tip-induced oxidation with  $\Delta U = 10 \text{ V}$  inside the square structures in (a). (c) Schematic representation of the structures in (b).

## 1.7

### Conclusion

In this chapter we discuss some selected aspects of electrocrystallization, which are relevant for a better understanding of both the nucleation and growth phenomena at an atomic level and the preparation of various nanostructures by electrochemical means. The presented examples demonstrate in how many respects the concepts of electrocrystallization affect the future development of nanotechnology. In particular this applies to the preparation of nanoparticles by controlled nucleation and growth, to the formation of atomic scale thin films and superlattices by underpotential deposition, to the fabrication of single- and polycrystalline nanowires by template electrodeposition and selective electrocrystallization at step edges and to the nanostructuring of metal and semiconductor substrates by SPM tip-induced electrocrystallization of metals and oxides.

## Acknowledgments

The authors gratefully acknowledge the financial support given by the Research Centre Jülich, the Bulgarian Academy of Sciences and the German Research Association (DFG).

## References

- 1 M. VOLMER, *Das elektrolytische Kristallwachstum*, Hermann et Cie, Paris, 1934.
- 2 M. VOLMER, *Kinetik der Phasenbildung*, Steinkopf, Dresden, 1939.
- 3 H. FISCHER, *Elektrolytische Abscheidung und Elektrokristallisation von Metallen*, Springer, Berlin, 1954.
- 4 J. O'M. BOCKRIS, G. A. RAZUMNEY, *Fundamental Aspects of Electrocrystallization*, Plenum Press, New York, 1967.
- 5 E. BUDEVSKI, G. STAIKOV, W. J. LORENZ, *Electrochemical Phase Formation and Growth – An Introduction to the Initial Stages of Metal Deposition*, VCH, Weinheim, 1996.
- 6 M. PAUNOVIC, M. SCHLESINGER, *Fundamentals of Electrochemical Deposition*, Wiley-Interscience, New York, 1998.
- 7 A. MILCHEV, *Electrocrystallization: Fundamentals of Nucleation and Growth*, Kluwer Academic Publishers, Boston/Dordrecht/London, 2002.
- 8 M. FLEISCHMANN, H. R. THIRSK, in *Advances in Electrochemistry and Electrochemical Engineering*, Vol. 3, P. DELAHAY (Ed.), Wiley, New York, 1963.
- 9 H. FISCHER, *Angew. Chem. Int. Ed. Engl.* 1969, 8, 108.
- 10 J. O'M. BOCKRIS, A. R. DESPIC, in *Physical Chemistry – An Advanced Treatise*, Vol. IXB, H. EYRING, D. HENDERSON, W. JOST (Eds.), Academic Press, New York, 1970.
- 11 D. M. KOLB, in *Advances in Electrochemistry and Electrochemical Engineering*, Vol. 11, H. GERISCHER, C. W. TOBIAS (Eds.), Wiley, New York, 1978.
- 12 E. BUDEVSKI, V. BOSTANOV, G. STAIKOV, *Annu. Rev. Mater. Sci.* 1980, 10, 85.
- 13 E. BUDEVSKI, in *Comprehensive Treatise of Electrochemistry*, Vol. 7, B. E. CONWAY, J. O'M. BOCKRIS, E. YEAGER, S. U. M. KAHN, R. E. WHITE (Eds.), Plenum Press, New York, 1983.
- 14 B. SCHARIFKER, G. HILLS, *Electrochim. Acta* 1983, 28, 879.
- 15 A. MILCHEV, *Contemp. Phys.* 1991, 32, 321.
- 16 P. ALLONGUE, in *Modern Aspects of Electrochemistry*, Vol. 23, B. E. CONWAY, J. O'M. BOCKRIS, R. E. WHITE (Eds.), Plenum Press, New York, 1992.
- 17 E. MICHAILOVA, I. VITANOVA, D. STOYCHEV, A. MILCHEV, *Electrochim. Acta* 1993, 38, 2455.
- 18 A. I. DANILOV, E. B. MOLODKINA, YU. M. POLUKAROV, *Russ. J. Electrochem.* 1994, 30, 674.
- 19 M. H. HÖLZLE, V. ZWING, D. M. KOLB, *Electrochim. Acta* 1995, 40, 1237.
- 20 G. OSKAM, J. G. LONG, A. NATARAJAN, P. C. SEARSON, *J. Phys. D: Appl. Phys.* 1998, 31, 1927.
- 21 E. BUDEVSKI, G. STAIKOV, W. J. LORENZ, *Electrochim. Acta* 2000, 45, 2499.
- 22 R. KRUMM, B. GUEL, C. SCHMITZ, G. STAIKOV, *Electrochim. Acta* 2000, 45, 3255.
- 23 G. STAIKOV, in *Electrochemical Microsystem Technologies*, J. W. SCHULTZE, T. OSAKA, M. DATTA (Eds.), Taylor & Francis, London and New York, 2002.
- 24 K. MÁRQUEZ, G. STAIKOV, J. W. SCHULTZE, *Electrochim. Acta* 2003, 48, 875.
- 25 A. MILCHEV, T. ZAPRYANOVA, *Electrochim. Acta* 2006, 51, 2926.

- 26 P. C. ANDRICACOS, C. UZOH, J. O. DUKOVIC, J. HORKANS, H. DELIGIANNI, *IBM J. Res. Develop.* **1998**, *42*, 567.
- 27 P. C. ANDRICACOS, *Interface* **1999**, *8*, 32.
- 28 A. BRENNER, *Electrodeposition of Alloys*, Academic Press, New York, **1963**.
- 29 K. M. GORBUNOVA, YU. M. POLUKAROV, in *Advances in Electrochemistry and Electrochemical Engineering*, Vol. 5, P. DELAHAY (Ed.), Wiley, New York, **1967**.
- 30 F. A. KRÖGER, *J. Electrochem. Soc.* **1978**, *125*, 2028.
- 31 P. C. ANDRICACOS, C. ARANA, J. TABIB, J. DUKOVIC, L. T. ROMANKIW, *J. Electrochem. Soc.* **1989**, *136*, 1336.
- 32 A. MILCHEV, R. LACMANN, *J. Cryst. Growth* **1991**, *110*, 919, 925.
- 33 K. RAJESHWAR, *Adv. Mater.* **1992**, *4*, 23.
- 34 D. LANDOLT, *Electrochim. Acta* **1994**, *39*, 1075.
- 35 G. HODES, in *Physical Electrochemistry*, I. RUBINSTEIN (Ed.), Marcel Dekker, New York, **1995**.
- 36 E. MICHAILOVA, A. MILCHEV, R. LACMANN, *Electrochim. Acta* **1996**, *41*, 329.
- 37 A. MILCHEV, *Electrochim. Acta* **1997**, *42*, 1533.
- 38 A. MILCHEV, E. MICHAILOVA, T. ZAPRYANOVA, *Electrochem. Commun.* **2004**, *6*, 713.
- 39 A. MILCHEV, G. STAIKOV, *Indian J. Chem.* **2005**, *44A*, 899.
- 40 L. YOUNG, *Anodic Oxide Films*, Academic Press, London, **1961**.
- 41 D. A. VERMILYEA, in *Advances in Electrochemistry and Electrochemical Engineering*, Vol. 3, P. DELAHAY (Ed.), Wiley, New York, **1963**.
- 42 M. J. DIGNAM, in *Comprehensive Treatise of Electrochemistry*, Vol. 4, J. O'M. BOCKRIS, B. E. CONWAY, E. YEAGER, R. E. WHITE (Eds.), Plenum Press, New York, **1981**.
- 43 M. FLEISCHMANN, L. J. LI, L. M. PETER, *Electrochim. Acta* **1989**, *34*, 475.
- 44 B. E. CONWAY, B. BARNETT, H. ANGERSTEIN-KOZLOWSKA, B. V. TILAK, *J. Chem. Phys.* **1990**, *93*, 8361.
- 45 J. W. SCHULTZE, M. M. LOHRENGEL, *Electrochim. Acta* **2000**, *45*, 2499.
- 46 H. BLOES, G. STAIKOV, J. W. SCHULTZE, *Electrochim. Acta* **2001**, *47*, 335.
- 47 V. LEHMANN, *Electrochemistry of Silicon: Instrumentation, Science, Materials and Applications*, Wiley-VCH, Weinheim, **2002**.
- 48 G. BINNIG, H. ROHRER, *Helv. Phys. Acta* **1982**, *55*, 726.
- 49 P. LUSTENBERGER, H. ROHRER, R. CHRISTOPH, H. SIEGENTHALER, *J. Electroanal. Chem.* **1988**, *243*, 225.
- 50 H. SIEGENTHALER, in *Scanning Tunneling Microscopy II*, Springer Ser. Surf. Sci., Vol. 28, R. WIESENDANGER, H.-J. GÜNTHERODT (Eds.), Springer, Berlin, **1992**.
- 51 G. STAIKOV, K. JÜTTNER, W. J. LORENZ, E. BUDEVSKI, *Electrochim. Acta* **1994**, *39*, 1019.
- 52 A. A. GEWIRTH, H. SIEGENTHALER (Eds.), *Nanoscale Probes of the Solid/Liquid Interface*, Kluwer Academic Publishers, Dordrecht/Boston/London, **1995**.
- 53 P. ALLONGUE, in *Advances in Electrochemical Science and Engineering*, Vol. 4, H. GERISCHER, C. W. TOBIAS (Eds.), VCH, Weinheim, **1995**.
- 54 W. PLIETH, W. J. LORENZ (Eds.), *Electrochemical Nanotechnology*, Wiley-VCH, Weinheim, **1998**.
- 55 K. ITAYA, *Prog. Surf. Sci.* **1998**, *58*, 121.
- 56 G. STAIKOV, W. J. LORENZ, E. BUDEVSKI, in *Imaging of Surfaces and Interfaces (Frontiers in Electrochemistry*, Vol. 5), J. LIPKOWSKI, P. N. ROSS (Eds.), Wiley-VCH, New York, **1999**.
- 57 R. J. NICHOLS, in *Imaging of Surfaces and Interfaces (Frontiers in Electrochemistry*, Vol. 5), P. N. ROSS, J. LIPKOWSKI (Eds.), Wiley-VCH, New York, **1999**.
- 58 T. P. MOFFAT, in *Electroanalytical Chemistry*, Vol. 21, A. J. BARD, I. RUBINSTEIN (Eds.), Marcel Dekker, New York, **1999**.
- 59 D. M. KOLB, *Electrochim. Acta* **2000**, *45*, 2387.
- 60 D. M. KOLB, in *Advances in Electrochemical Science and Engineering*, Vol. 7, R. C. ALKIRE, D. M. KOLB (Eds.), Wiley-VCH, Weinheim, **2001**.

- 61 J. L. STICKNEY, in *Advances in Electrochemical Science and Engineering*, Vol. 7, R. C. ALKIRE, D. M. KOLB (Eds.), Wiley-VCH, Weinheim, 2001.
- 62 D. P. BARKEY, in *Advances in Electrochemical Science and Engineering*, Vol. 7, R. C. ALKIRE, D. M. KOLB (Eds.), Wiley-VCH, Weinheim, 2001.
- 63 W. J. LORENZ, G. STAIKOV, W. SCHINDLER, W. WIESBECK, *J. Electrochem. Soc.* **2002**, 149, K47.
- 64 W. POLEWSKA, R. J. BEHM, O. M. MAGNUSSEN, *Electrochim. Acta* **2003**, 48, 2915.
- 65 W. FREYLAND, C. A. ZELL, S. ZEIN EL ABEDIN, F. ENDRES, *Electrochim. Acta* **2003**, 48, 3053.
- 66 A. MILCHEV, *J. Electroanal. Chem.*, **1998**, 457, 35.
- 67 A. MILCHEV, *J. Electroanal. Chem.*, **1998**, 457, 47.
- 68 A. MILCHEV, E. MICHAILOVA, *Electrochem. Commun.*, **2000**, 2, 15.
- 69 R. T. PÖTZSCHKE, G. STAIKOV, W. J. LORENZ, W. WIESBECK, *J. Electrochem. Soc.*, **1999**, 146, 141.
- 70 W. SCHINDLER, D. HOFMANN, J. KIRSCHNER, *J. Electrochem. Soc.*, **2001**, 148, C124.
- 71 W. SCHINDLER, P. HUGELMANN, M. HUGELMANN, F. X. KÄRTNER, *J. Electroanal. Chem.*, **2002**, 522, 49.
- 72 R. WIDMER, H. SIEGENTHALER, *Electrochem. Commun.*, **2005**, 7, 421.
- 73 A. MILCHEV, S. STOYANOV, *J. Electroanal. Chem.*, **1976**, 72, 33.
- 74 S. STOYANOV, in *Current Topics in Materials Science*, Vol. 3, E. KALDIS (Ed.), North-Holland, Amsterdam, 1978.
- 75 J. MOSTANY, J. PARRA, B. R. SCHARIFKER, *J. Appl. Electrochem.*, **1986**, 16, 333.
- 76 A. SERRUYA, B. R. SCHARIFKER, I. GONZALEZ, M. T. OROPEZA, M. PALOMAR-PARDAVE, *J. Appl. Electrochem.*, **1996**, 26, 451.
- 77 M. PALOMAR-PARDAVE, M. TERESA RAMIREZ, I. GONZALEZ, A. SERRUYA, B. R. SCHARIFKER, *J. Electrochem. Soc.*, **1996**, 143, 1551.
- 78 A. KELAIDPOULOU, G. KOKKINIDIS, A. MILCHEV, *J. Electroanal. Chem.* **1998**, 444, 195.
- 79 A. SERRUYA, J. MOSTANY, B. R. SCHARIFKER, *J. Electroanal. Chem.*, **1999**, 464, 39.
- 80 A. MILCHEV, D. STOYCHEV, V. LAZAROV, A. PAPOUTSIS, G. KOKKINIDIS, *J. Cryst. Growth*, **2001**, 226, 138.
- 81 M. ARBIB, B. ZHANG, V. LAZAROV, D. STOYCHEV, A. MILCHEV, C. BUSSHERMAN, *J. Electroanal. Chem.*, **2001**, 510, 67.
- 82 L. H. MENDOZA-HUIZAR, J. ROBLES, M. PALOMAR-PARDAVE, *J. Electroanal. Chem.*, **2002**, 521, 95.
- 83 L. H. MENDOZA-HUIZAR, J. ROBLES, M. PALOMAR-PARDAVE, *J. Electroanal. Chem.*, **2003**, 545, 39.
- 84 L. H. MENDOZA-HUIZAR, J. ROBLES, M. PALOMAR-PARDAVE, *J. Electrochem. Soc.*, **2005**, 152, 95.
- 85 R. BECKER, W. DÖRING, *Ann. Phys.*, **1935**, 24, 719.
- 86 Ya. B. ZELDOVICH, *Acta Physicochim. USSR*, **1943**, 18, 1.
- 87 A. MILCHEV, S. STOYANOV, R. KAISCHEW, *Thin Solid Films*, **1974**, 22, 255, 267.
- 88 P. HERTZ, *Math. Ann.*, **1909**, 67, 387.
- 89 S. CHANDRASEKHAR, *Rev. Mod. Phys.*, **1943**, 15, 1.
- 90 A. MILCHEV, *J. Chem. Phys.*, **1994**, 100, 5160.
- 91 A. MILCHEV, E. MICHAILOVA, I. LESIGIRASKA, *Electrochem. Commun.*, **2000**, 2, 407.
- 92 W. S. KRUIJT, M. SLUYTERS-REHBACH, J. H. SLUYTERS, A. MILCHEV, *J. Electroanal. Chem.*, **1994**, 371, 13.
- 93 J. MOSTANY, A. SERRUYA, B. R. SCHARIFKER, *J. Electroanal. Chem.*, **1995**, 383, 33.
- 94 U. SCHMIDT, M. DONTEN, J. G. OSTERYOUNG, *J. Electrochem. Soc.*, **1997**, 144, 2013.
- 95 S. IVANOV, V. TSAKOVA, *J. Appl. Electrochem.*, **2002**, 32, 709.
- 96 A. MILCHEV, W. S. KRUIJT, M. SLUYTERS-REHBACH, J. H. SLUYTERS, *J. Electroanal. Chem.*, **1993**, 362, 21.
- 97 V. TSAKOVA, A. MILCHEV, *J. Electroanal. Chem.*, **1998**, 451, 211.
- 98 S. FLETCHER, *J. Cryst. Growth*, **1983**, 62, 505.
- 99 A. MILCHEV, *J. Appl. Electrochem.*, **1990**, 20, 307.

- 100 A. MILCHEV, *J. Electroanal. Chem.*, **1991**, 312, 267.
- 101 A. MILCHEV, L. HEERMAN, *Electrochim. Acta*, **2003**, 48, 2903.
- 102 G. GUNAWARDENA, G. HILLS, I. MONTENEGRO, B. SCHARIFKER, *J. Electroanal. Chem.*, **1982**, 138, 225.
- 103 B. R. SCHARIFKER, J. MOSTANY, *J. Electroanal. Chem.*, **1984**, 177, 13.
- 104 M. V. MIRKIN, A. P. NILOV, *J. Electroanal. Chem.*, **1990**, 283, 35.
- 105 L. HEERMAN, A. TARALLO, *J. Electroanal. Chem.*, **1999**, 470, 70.
- 106 L. HEERMAN, E. MATTHIJS, S. LANGEROCK, *Electrochim. Acta*, **2000**, 47, 905.
- 107 H. LIU, F. FAVIER, K. NG, M. P. ZACH, R. M. PENNER, *Electrochim. Acta*, **2001**, 47, 671.
- 108 R. M. PENNER, *J. Phys. Chem. B*, **2002**, 106, 3339.
- 109 K. MÁRQUEZ, G. STAIKOV, J. W. SCHULTZE, *Trans. IMF*, **2002**, 80, 73.
- 110 K. MÁRQUEZ, R. ORTIZ, J. W. SCHULTZE, O. P. MÁRQUEZ, J. MÁRQUEZ, G. STAIKOV, *Electrochim. Acta*, **2003**, 48, 711.
- 111 D. CARNAL, P. I. ODEN, U. MÜLLER, E. SCHMIDT, H. SIEGENTHALER, *Electrochim. Acta*, **1995**, 40, 1223.
- 112 G. STAIKOV, in *Nanoscale Probes of the Solid/Liquid Interface*, A. A. GEWIRTH, H. SIEGENTHALER (Eds.), Kluwer Academic Publishers, Dordrecht/Boston/London, **1995**.
- 113 U. SCHMIDT, S. VINZELBERG, G. STAIKOV, *Surf. Sci.*, **1996**, 348, 261.
- 114 G. STAIKOV, W. J. LORENZ, *Can. J. Chem.*, **1997**, 75, 1624.
- 115 J. SACKMANN, A. BUNK, R. T. PÖTZSCHKE, G. STAIKOV, W. J. LORENZ, *Electrochim. Acta*, **1998**, 43, 2863.
- 116 S. GARCIA, D. SALINAS, C. MAYER, E. SCHMIDT, G. STAIKOV, W. J. LORENZ, *Electrochim. Acta*, **1998**, 43, 3007.
- 117 G. STAIKOV, W. J. LORENZ, *Z. Phys. Chem.*, **1999**, 208, 17.
- 118 S.-J. HSIEH, A. A. GEWIRTH, *Langmuir*, **2000**, 9501.
- 119 R. VIDU, S. HARA, *Surf. Sci.*, **2000**, 452, 229.
- 120 R. WIDMER, H. SIEGENTHALER, *J. Electrochem. Soc.*, **2004**, 151, E238.
- 121 S. GARCIA, D. R. SALINAS, G. STAIKOV, *Surf. Sci.*, **2005**, 576, 9.
- 122 J. L. STICKNEY, in *Electroanalytical Chemistry*, Vol. 21, A. J. BARD, I. RUBINSTEIN (Eds.), Marcel Dekker, New York, **1999**.
- 123 H. J. PAULING, K. JÜTTNER, *Electrochim. Acta*, **1992**, 37, 2237.
- 124 H. J. PAULING, G. STAIKOV, K. JÜTTNER, *J. Electroanal. Chem.*, **1994**, 376, 179.
- 125 K. SIERADZKI, S. R. BRANKOVICH, N. DIMITROV, *Science*, **1999**, 284, 138.
- 126 S. R. BRANKOVICH, N. DIMITROV, K. SIERADZKI, *Electrochem. Solid-State Lett.*, **1999**, 2, 443.
- 127 D. JOSELL, C. R. BEAUCHAMP, D. R. KELLEY, C. A. WITT, T. P. MOFFAT, *Electrochem. Solid-State Lett.*, **2005**, 8, C54.
- 128 D. JOSELL, D. WHEELER, T. P. MOFFAT, *J. Electrochem. Soc.*, **2006**, 153, C11.
- 129 K. SASAKI, Y. MO, J. X. WANG, M. BALASUBRAMANIAN, F. URIBE, J. MCBREEN, R. R. ADZIC, *Electrochim. Acta*, **2003**, 48, 3841.
- 130 J. ZHANG, Y. MO, M. B. VUKMIROVIC, R. KLIE, K. SASAKI, R. R. ADZIC, *J. Phys. Chem. B*, **2004**, 108, 10995.
- 131 L. KOMSIYSKA, G. STAIKOV, unpublished results.
- 132 J. ZHANG, F. H. B. LIMA, M. H. SHAO, K. SASAKI, J. X. WANG, J. HANSON, R. R. ADZIC, *J. Phys. Chem. B*, **2005**, 109, 22701.
- 133 J. O. DUKOVIC, in *Advances in Electrochemical Science and Engineering*, Vol. 3, H. GERISCHER, C. W. TOBIAS (Eds.), VCH, Weinheim, **1994**.
- 134 C. R. MARTIN, *Science*, **1994**, 266, 1961.
- 135 G. YI, W. SCHWARZACHER, *Appl. Phys. Lett.*, **1999**, 74, 1746.
- 136 T. W. CORNELIUS, J. BRÖTZ, N. CHTANKO, D. DOBREV, G. MIEHE, R. NEUMANN, M. E. TOIMIL MOLARES, *Nanotechnology*, **2005**, 16, S246.
- 137 E. C. WALTER, B. J. MURRAY, F. FAVIER, G. KALTENPOTH, M. GRUNZE, R. M. PENNER, *J. Phys. Chem. B*, **2002**, 106, 11407.

- 138 Q. LI, J. T. NEWBERG, E. C. WALTER, J. C. HEMMINGER, R. M. PENNER, *Nano Lett.*, **2004**, 4, 277.
- 139 E. J. MENKE, Q. LI, R. M. PENNER, *Nano Lett.*, **2004**, 4, 2009.
- 140 A. HEIDELBERG, C. ROZENKRANZ, J. W. SCHULTZE, Th. SCHÄPERS, G. STAIKOV, *Surf. Sci.*, **2005**, 597, 173.
- 141 J. W. SCHULTZE, A. HEIDELBERG, C. ROZENKRANZ, Th. SCHÄPERS, G. STAIKOV, *Electrochim. Acta*, **2005**, 51, 775.
- 142 H. BLOESS, PhD Thesis, University of Düsseldorf, **2002**.
- 143 J. A. DAGATA, J. SCHNEIR, H. H. HARARY, C. J. EVANS, M. T. POSTEK, J. BENNET, *Appl. Phys. Lett.*, **1990**, 56, 2001.
- 144 H. SUGIMURA, T. UCHIDA, N. KITAMURA, H. MASUHARA, *Appl. Phys. Lett.*, **1993**, 63, 1288.
- 145 J. A. DAGATA, T. INOUE, J. ITOH, K. MATSUMOTO, H. YOKOYAMA, *J. Appl. Phys.*, **1998**, 84, 6891.
- 146 E. DUBOIS, J. L. BUBENDORFF, *J. Appl. Phys.*, **2000**, 87, 8148.
- 147 E. S. SNOW, G. G. JEMIGAN, P. M. CAMPBELL, *Appl. Phys. Lett.*, **2000**, 76, 1782.
- 148 N. FARKAS, G. ZHANG, E. A. EVANS, R. D. RAMSIER, J. A. DAGATA, *J. Vac. Sci. Technol. A*, **2003**, 21, 1188.